Hybrid stars in the quark-meson coupling model with superconducting quark matter

P. K. Panda and D. P. Menezes
Departamento de Física, CFM, Universidade Federal de Santa Catarina, Caixa Postal 476, 88040 900 Florianópolis—SC, Brazil

C. Providência
Centro de Física Teórica, Departamento de Física, Universidade de Coimbra, P-3004-516 Coimbra, Portugal
(Received 26 September 2003; published 27 February 2004)

The phase transition to a deconfined phase is studied and the consequences in the formation of neutron stars are investigated. We use the quark-meson coupling model for the hadron matter and the MIT bag model for the quark matter in order to build the appropriate equations of state for the hybrid stars. The properties of the stars are then calculated. The differences between unpaired and color-flavor locked quark matter are discussed.

DOI: 10.1103/PhysRevC.69.025207 PACS number(s): 95.30.Tg, 21.65.+f, 12.39.Ba, 21.30.−x

I. INTRODUCTION

It is widely believed that hadronic matter undergoes a phase transition to quark matter at high densities and/or high temperatures. The high temperature limit is important in heavy ion collisions and/or cosmology, whereas the high baryon density behavior is important for the study of neutron, hybrid, and quark stars.

After a gravitational collapse of a massive star takes place, a neutron star with practically zero temperature can be born few seconds after deleptonization. The correct calculations of the star properties depend on the appropriate equations of state (EOS) that describe its crust and interior. The crust of the neutron star, where density is low, is believed to be adequately described by hadronic matter. Its interior, however, where density is of the order of five to ten times nuclear saturation density, remains to be properly understood. Whether the central part of the star is composed of quark matter only, of mixed matter, or of paired quark matter is one of the subjects of the present work.

In the present paper we are interested in building the EOS for mixed matter of quark and hadron phases. We employ the quark-meson coupling model (QMC) [1,2] including hyperons in order to describe the hadron phase. In the QMC model, baryons are described as a system of nonoverlapping MIT bags which interact through the effective scalar and vector mean fields, very much in the same way as in the Walecka model [quantum hadrodynamics (QHD)] [3]. Many applications and extensions of the model have been made in the last years [4–10].

While the QMC model shares many similarities with QHD-type models, it however offers new opportunities for studying nuclear matter properties. One of the most attractive aspects of the model is that different phases of hadronic matter, from very low to very high baryon densities and temperatures, can be described within the same underlying model, namely, the MIT bag model. In the QMC, matter at low densities and temperatures is a system of nucleons interacting through meson fields, with quarks and gluons confined within MIT bag. For matter at very high density and/or temperature, one expects that baryons and mesons dissolve and the entire system of quarks and gluons becomes confined within a single, big MIT bag. Another important aspect of the QMC is that the internal structure of the nucleon is introduced explicitly. It is found that the EOS for infinite nuclear matter at zero temperature derived from the QMC model is much softer than the one obtained in the Walecka model [3]. Also, the QMC model nucleon effective mass lies in the range 0.7–0.8 of the free nucleon mass, which agrees with results derived from nonrelativistic analysis of scattering of neutrons from lead nuclei [11] and is larger in comparison with Walecka model effective mass. Consequently, we expect that contrary to the NL3 and TM1 parametrizations of the nonlinear Walecka model (NLWM) with hyperons, the mass of the nucleon does not become zero at densities $\rho < 10\rho_0, \rho_0$ being the density of nuclear matter at saturation. At finite temperature, there arises yet another difference between predictions of QMC and QHD, namely, the behavior of the effective nucleon mass with the temperature at fixed baryon density. While in QHD-type models the nucleon mass always decreases with temperature, in the QMC it increases. The difference arises because of the explicit treatment of the internal structure of the nucleon in the QMC. When the bag is heated up, quark-antiquark pairs are excited in the interior of the bag, increasing the internal energy of the bag [8]. In what follows we consider the QMC with a constant bag constant, e.g., not dependent on the scalar meson field as in the modified quark-meson coupling models (MQMC) [9,10]. Contrary to the QMC result, the bag radius increases with density for all MQMC models with a meson dependent bag constant [10]. For densities not much larger than nuclear matter saturation density ρ_0 the bags start to overlap which implies a breakdown of the model. In the present work we are interested in describing the properties of nuclear matter for densities which go beyond the saturation density, and therefore have chosen to consider the QMC model.

For the quark phase we have chosen to use both unpaired quark matter (UQM) described by the MIT bag model [12–15] and paired quarks described by the color-flavor locked (CFL) phase. Recently many authors [16–21] have discussed the possibility that the quark matter is in a color-superconducting phase, in which quarks near the Fermi surface are paired, forming Cooper pairs which condense and break the color gauge symmetry [22]. At sufficiently high density the favored phase is called CFL, in which quarks of all three colors and all three flavors are allowed to pair.

 ©2004 The American Physical Society

Once the mixed EOS is built by enforcing appropriate Gibbs criteria and chemical equilibrium conditions, the properties of the stars are calculated and discussed. We have restricted ourselves to the investigation of neutron stars ($T=0$) at least a couple of minutes old where the effects of finite temperature and neutrino trapping are not important [23,24].

In recent works [25,26], two of us have studied the properties of mixed stars whose equations of state were built with the NLWM for the hadron matter [3] and the MIT bag [12–15], and the Nambu–Jona-Lasinio [27] models for the unpaired quark matter. In the first work [25] the effects of temperature were investigated and in the second one the consequences of imposing neutrino trapping at fixed entropies were studied. In both works, only in very special cases, the interior of the stars was made of quarks only. In general, a mixed phase of hadrons and quarks was favored.

In what follows we compare the properties of neutron stars obtained within the QMC model with hyperons and with both quark models discussed above, namely, the onset of hyperons, mixed and quark phases, strangeness content, the maximum allowed masses, and core composition.

The present paper is organized as follows: in Sec. II the QMC model with hyperons is reviewed. In Secs. III and IV the unpaired quark matter and the CFL phase are described. In Sec. V the mixed phase is implemented, and the results are shown and discussed in Sec. VI. Finally, in the last section, the conclusions are drawn.

II. THE QUARK-MESON COUPLING MODEL FOR HADRONIC MATTER

In the QMC model, the nucleon in nuclear medium is assumed to be a static spherical MIT bag in which quarks interact with the scalar and vector fields, σ, ω, and ρ, and these fields are treated as classical fields in the mean-field approximation. The quark field $\psi_q(x)$ inside the bag then satisfies the following equation of motion:

$$\left[i\partial\!\!\!/ - (m_q^0 - g_\sigma^q\sigma) - g_\omega^q\omega\gamma^0 + \tfrac{1}{2}g_\rho^q\tau_z\rho_{03}\right]\psi_q(x) = 0, \quad q = u,d,s, \tag{2.1}$$

where m_q^0 is the current quark mass, and g_σ^q, g_ω^q, and g_ρ^q denote the quark-meson coupling constants. The normalized ground state for a quark in the bag is given by [1,2]

$$\psi_q(\mathbf{r},t) = \mathcal{N}_q \exp(-i\epsilon_q t/R_B)\begin{pmatrix} j_0(x_q r/R_B) \\ i\beta_q\vec{\sigma}\cdot\hat{r}j_1(x_q r/R_B)\end{pmatrix}\frac{\chi_q}{\sqrt{4\pi}}, \tag{2.2}$$

where

$$\epsilon_q = \Omega_q + R_B\left(g_\omega^q\omega + \tfrac{1}{2}g_\rho^q\tau_z\rho_{03}\right); \quad \beta_q = \sqrt{\frac{\Omega_q - R_B m_q^*}{\Omega_q + R_B m_q^*}}, \tag{2.3}$$

with the normalization factor given by

TABLE I. Bag constants for the baryons at the free space value $B_B^{1/4}$. The third and fourth columns are obtained for $B_B^{1/4}=210.854$ and the mass of the quarks taken as $m_u=m_d=5.5$ MeV and $m_s=150$ MeV. The last two columns are for $B_B^{1/4}=211.303$ and the mass of the quarks taken as $m_u=m_d=0$ MeV and $m_s=150$ MeV.

Baryons	M_B	Z_B	R_B	Z_B	R_B
N	939.0	4.00506	0.6	3.98699	0.6
Λ	1115.6	3.69005	0.62525	3.68029	0.62428
Σ^+	1189.3	3.45577	0.63977	3.44628	0.63870
Σ^0	1192.5	3.40386	0.64038	3.43600	0.63931
Σ^-	1197.4	3.42970	0.64038	3.42024	0.64024
Ξ^0	1314.9	3.29260	0.65336	3.29188	0.65182
Ξ^-	1321.3	3.27173	0.65455	3.27105	0.65301

$$\mathcal{N}_q^{-2} = 2R_B^3 j_0^2(x_q)[\Omega_q(\Omega_q - 1) + R_B m_q^*/2]/x_q^2, \tag{2.4}$$

where $\Omega_q \equiv \sqrt{x_q^2 + (R_B m_q^*)^2}$, $m_q^* = m_q^0 - g_\sigma^q\sigma$, R_B is the bag radius of the baryon, and χ_q is the quark spinor. The quantities $\psi_q, \epsilon_q, \beta_q, \mathcal{N}_q, \Omega_q, m_q^*$ all depend on the baryon considered. The bag eigenvalue x_q is determined by the boundary condition at the bag surface

$$j_0(x_q) = \beta_q j_1(x_q). \tag{2.5}$$

The energy of a static bag describing baryon B consisting of three ground state quarks can be expressed as

$$E_B^{\text{bag}} = \sum_q n_q\frac{\Omega_q}{R_B} - \frac{Z_B}{R_B} + \frac{4}{3}\pi R_B^3 B_B, \tag{2.6}$$

where Z_B is a parameter which accounts for zero-point motion and B_B is the bag constant. The set of parameters used in the present work is given in Table I. The effective mass of a nucleon bag at rest is taken to be

$$M_B^* = E_B^{\text{bag}}. \tag{2.7}$$

The equilibrium condition for the bag is obtained by minimizing the effective mass M_B^* with respect to the bag radius,

$$\frac{d\,M_B^*}{d\,R_B} = 0. \tag{2.8}$$

For the QMC model, the equations of motion for the meson fields in uniform static matter are given by

$$m_\sigma^2\sigma = \sum_B g_{\sigma B}C_B(\sigma)\frac{2J_B+1}{2\pi^2}\int_0^{k_B}\frac{M_B^*(\sigma)}{[k^2 + M_B^{*2}(\sigma)]^{1/2}}k^2dk, \tag{2.9}$$

$$m_\omega^2\omega_0 = \sum_B g_{\omega B}(2J_B+1)k_B^3/(6\pi^2), \tag{2.10}$$

$$m_\rho^2\rho_{03} = \sum_B g_{\rho B}I_{3B}(2J_B+1)k_B^3/(6\pi^2). \tag{2.11}$$

In the above equations J_B, I_{3B}, and k_B are, respectively, the spin, isospin projection, and the Fermi momentum of the baryon species B. The hyperon couplings are not relevant to the ground state properties of nuclear matter, but information about them can be available from the levels in Λ hypernuclei [28]. Here

$$g_{\sigma B} = x_{\sigma B} g_{\sigma N}, \quad g_{\omega B} = x_{\omega B} g_{\omega N}, \quad g_{\rho B} = x_{\rho B} g_{\rho N}$$

and $x_{\sigma B}$, $x_{\omega B}$, and $x_{\rho B}$ are equal to 1 for the nucleons and acquire different values in different parametrizations for the other baryons. Note that the s quark is unaffected by the σ and ω mesons, i.e., $g_\sigma^s = g_\omega^s = 0$.

In Eq. (2.9) we have

$$g_{\sigma B} C_B(\sigma) = -\frac{\partial M_B^*(\sigma)}{\partial \sigma} = -\frac{\partial E_B^{\rm bag}}{\partial \sigma} = \sum_{q=u,d} n_q g_\sigma^q S_B(\sigma), \tag{2.12}$$

where

$$S_B(\sigma) = \int_{bag} d\mathbf{r}\, \overline{\psi}_q \psi_q = \frac{\Omega_q/2 + R_B m_q^*(\Omega_q - 1)}{\Omega_q(\Omega_q - 1) + R_B m_q^*/2}, \quad q \equiv (u,d). \tag{2.13}$$

The total energy density and the pressure including the leptons can be obtained from the grand canonical potential and they read

$$\varepsilon = \frac{1}{2} m_\sigma^2 \sigma^2 + \frac{1}{2} m_\omega^2 \omega_0^2 + \frac{1}{2} m_\rho^2 \rho_{03}^2 + \sum_B \frac{2J_B + 1}{2\pi^2} \int_0^{k_B} k^2 dk [k^2 + M_B^{*2}(\sigma)]^{1/2} + \sum_l \frac{1}{\pi^2} \int_0^{k_l} k^2 dk [k^2 + m_l^2]^{1/2}, \tag{2.14}$$

$$P = -\frac{1}{2} m_\sigma^2 \sigma^2 + \frac{1}{2} m_\omega^2 \omega_0^2 + \frac{1}{2} m_\rho^2 \rho_{03}^2 + \frac{1}{3} \sum_B \frac{2J_B + 1}{2\pi^2} \int_0^{k_B} \frac{k^4 dk}{[k^2 + M_B^{*2}(\sigma)]^{1/2}} + \frac{1}{3} \sum_l \frac{1}{\pi^2} \int_0^{k_l} \frac{k^4 dk}{[k^2 + m_l^2]^{1/2}}. \tag{2.15}$$

The lepton Fermi momenta are the positive real solutions of $(k_e^2 + m_e^2)^{1/2} = \mu_e$ and $(k_\mu^2 + m_\mu^2)^{1/2} = \mu_\mu = \mu_e$. The equilibrium composition of the star is obtained by solving the set of Eqs. (2.9)–(2.11) in conjunction with the charge neutrality condition (2.16) at a given total baryonic density $\rho = \Sigma_B (2J_B + 1) k_B^3/(6\pi^2)$; the baryon effective masses are obtained self-consistently in the bag model.

For stars in which the strongly interacting particles are baryons, the composition is determined by the requirements of charge neutrality and β-equilibrium conditions under the weak processes $B_1 \to B_2 + l + \overline{\nu_l}$ and $B_2 + l \to B_1 + \nu_l$. After deleptonization, the charge neutrality condition yields

$$q_{\rm tot} = \sum_B q_B (2J_B + 1) k_B^3/(6\pi^2) + \sum_{l=e,\mu} q_l k_l^3/(3\pi^2) = 0, \tag{2.16}$$

where q_B corresponds to the electric charge of baryon species B and q_l corresponds to the electric charge of lepton species l. Since the time scale of a star is effectively infinite compared to the weak interaction time scale, weak interaction violates strangeness conservation. The strangeness quantum number is therefore not conserved in a star and the net strangeness is determined by the condition of β equilibrium which for baryon B is then given by $\mu_B = b_B \mu_n - q_B \mu_e$, where μ_B is the chemical potential of baryon B and b_B its baryon number. Thus the chemical potential of any baryon can be obtained from the two independent chemical potentials μ_n and μ_e of neutron and electron, respectively.

We start by fixing the free-space bag properties for the QMC model. For the bag radius $R_N = 0.6$, we first fixed the two unknowns Z_N and B_N for nucleons. These are obtained by fitting the nucleon mass $M = 939$ MeV and enforcing the stability condition for the bag at free space. The values obtained are $Z_N = 3.986\ 99$ and $B_N^{1/4} = 211.303$ MeV for $m_u = m_d = 0$ MeV and $Z_N = 4.005\ 06$ and $B_N^{1/4} = 210.854$ MeV for $m_u = m_d = 5.5$ MeV. We then fixed these bag values B_B for all baryons, and the parameter Z_B and R_B of the other baryons are obtained by reproducing their physical masses in free space and again enforcing the stability condition for their bags. The values obtained for Z_B and R_B are displayed in Table I for $m_u = m_d = 0$ MeV and for $m_u = m_d = 5.5$ MeV. Note that for a fixed bag value, the equilibrium condition in free space results in an increase of the bag radius and a decrease of the parameters Z_B for the heavier baryons.

Next we fit the quark-meson coupling constants , $g_\sigma^q, g_\omega = 3g_\omega^q$, and $g_\rho = g_\rho^q$ for the nucleon to obtain the correct saturation properties of the nuclear matter, $E_B \equiv \epsilon/\rho - M = -15.7$ MeV at $\rho = \rho_0 = 0.15$ fm^{-3}, $a_{sym} = 32.5$ MeV, $K = 257$ MeV, and $M^* = 0.774M$. We have $g_\sigma^q = 5.957$, $g_{\omega N} = 8.981$, and $g_{\rho N} = 8.651$. We take the standard values for the meson masses: $m_\sigma = 550$ MeV, $m_\omega = 783$ MeV, and $m_\rho = 770$ MeV.

For the meson-hyperon coupling constants we have opted for three sets discussed in the literature: set (a), based on quark counting arguments we take $x_{\sigma B} = x_{\omega B} = x_{\rho B} = \sqrt{2/3}$ as in Ref. [29]; set (b), according to Ref. [30,31] we choose the hyperon coupling constants constrained by the binding of the Λ hyperon in nuclear matter, hypernuclear levels, and neutron star masses ($x_\sigma = 0.7$ and $x_\omega = x_\rho = 0.783$) and assume that the couplings to the Σ and Ξ are equal to those of the Λ hyperon; set (c), based on the SU(6) symmetry for the light quarks (u,d) counting rule [5] we take $x_{\sigma B} = x_{\omega B} = 2/3$ and $x_{\rho\Lambda} = 0, x_{\rho\Sigma} = 2, x_{\rho\Xi} = 1$.

In Fig. 1 we have plotted the EOS obtained with the above parametrization of QMC and two choices of the hyperon couplings, sets (a) and (b) together with the corresponding EOS obtained with NLWM with cubic and quartic σ terms ($K = 300$ MeV and $M^* = 0.7M$). Although the NLWM-EOS is harder at low densities, it becomes softer at higher energies after the onset of the hyperons. This fact has consequences on the behavior of the mixed phase and on the

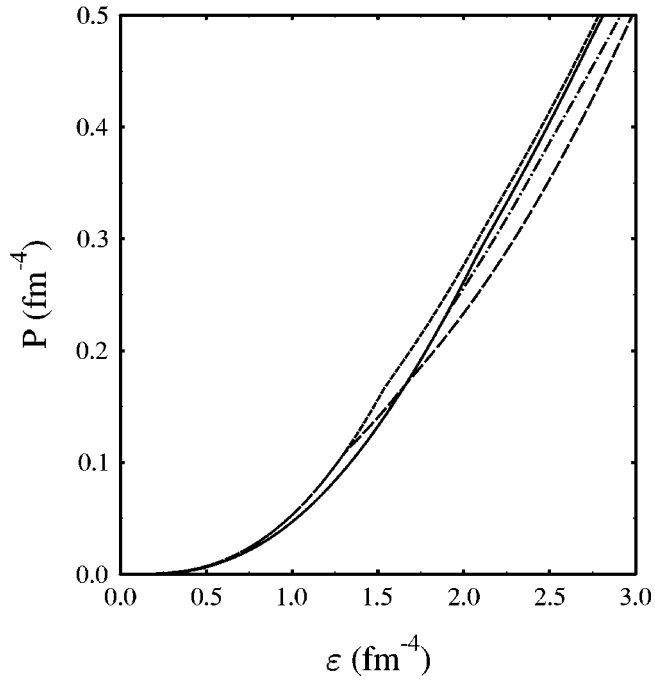

FIG. 1. EOS obtained with QMC and set (a) (solid line), QMC and set (b) (dot-dashed line), NLWM and set (a) (dashed line), and NLWM and set (b) (dotted line) including hyperons.

star properties. Moreover, one can see that different choices of the meson-hyperon parameters have a greater influence on the NLWM, for which the curves separate at lower densities and become more distant one from the other at high densities, than in the QMC.

III. UNPAIRED QUARK MATTER EQUATION OF STATE

The possible existence of quark matter in the core of neutron stars is an exciting possibility [13]. Densities of these stars are expected to be high enough to force the hadron constituents or nucleons to overlap, thereby yielding quark matter. We take the quark matter equation of state as in Refs. [14,15] in which u, d, and s quark degrees of freedom are included in addition to electrons. Up and down quark masses are set to 5.5 MeV and the strange quark mass is taken to be 150 MeV. In chemical equilibrium $\mu_d=\mu_s=\mu_u+\mu_e$. In terms of neutron and electric charge chemical potentials μ_n and μ_e, one has

$$\mu_u = \tfrac{1}{3}\mu_n - \tfrac{2}{3}\mu_e, \quad \mu_d = \tfrac{1}{3}\mu_n + \tfrac{1}{3}\mu_e, \quad \mu_s = \tfrac{1}{3}\mu_n + \tfrac{1}{3}\mu_e. \tag{3.1}$$

The pressure for quark flavor f, with $f=u,d$, or s is [15]

$$P_q = \frac{1}{4\pi^2}\sum_f \left[\mu_f k_f(\mu_f^2 - 2.5m_f^2) + 1.5m_f^4 \ln\left(\frac{\mu_f + k_f}{m_f}\right)\right], \tag{3.2}$$

where the Fermi momentum is $k_f=(\mu_f^2-m_f^2)^{1/2}$.

For the leptons, the pressure reads

$$P_l = \frac{1}{3\pi^2}\sum_l \int \frac{p^4 dp}{\sqrt{p^2+m_l^2}}. \tag{3.3}$$

The total pressure, including the bag constant B, which simulates confinement becomes

$$P = P_l + P_q - B. \tag{3.4}$$

There are only two independent chemical potentials μ_n and μ_e. μ_e is adjusted so that the matter is electrically neutral, i.e., $\partial P/\partial\mu_e=0$.

IV. COLOR-FLAVOR LOCKED QUARK PHASE

In this section we study the equation of state taking into consideration a CFL quark paired phase. We treat the quark matter as a Fermi sea of free quarks with an additional contribution to the pressure arising from the formation of the CFL condensates.

The CFL phase can be described with the help of the thermodynamical potential which reads [17]

$$\Omega_{CFL}(\mu_q,\mu_e) = \Omega_{quarks}(\mu_q) + \Omega_{GB}(\mu_q,\mu_e) + \Omega_l(\mu_e), \tag{4.1}$$

where $\mu_q=\mu_n/3$; and

$$\Omega_{quarks}(\mu_q) = \frac{6}{\pi^2}\int_0^\nu p^2 dp(p-\mu_q) + \frac{3}{\pi^2}\int_0^\nu p^2 dp(\sqrt{p^2+m_s^2} - \mu_q) - \frac{3\Delta^2\mu_q^2}{\pi^2} + B, \tag{4.2}$$

with $m_u=m_d$ set to zero,

$$\nu = 2\mu_q - \sqrt{\mu_q^2 + \frac{m_s^2}{3}}; \tag{4.3}$$

$\Omega_{GB}(\mu_q,\mu_e)$ is a contribution from the Goldstone bosons arising due to the chiral symmetry breaking in the CFL phase [17,32],

$$\Omega_{GB}(\mu_q,\mu_e) = -\frac{1}{2}f_\pi^2\mu_e^2\left(1 - \frac{m_\pi^2}{\mu_e^2}\right)^2, \tag{4.4}$$

where

$$f_\pi^2 = \frac{(21-8\ln 2)\mu_q^2}{36\pi^2}, \quad m_\pi^2 = \frac{3\Delta^2}{\pi^2 f_\pi^2} m_s(m_u+m_d); \tag{4.5}$$

$\Omega_l(\mu_e)$ is the negative of expression (3.3); and the quark number densities are equal, i.e.,

$$\rho_u = \rho_d = \rho_s = \frac{\nu^3 + 2\Delta^2\mu_q}{\pi^2}. \tag{4.6}$$

In the above expressions Δ, the gap parameter is taken to be 100 MeV [17].

The electric charge density carried by the pion condensate is given by

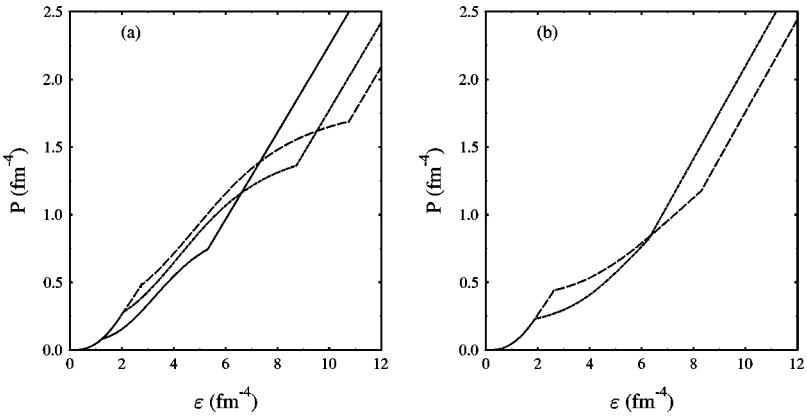

FIG. 2. EOS obtained with QMC plus UQM (a) for $B^{1/4}=180$ (solid line), 200 (short-dashed line), and 210.85 MeV (long-dashed line); and QMC plus CFL (b) for $B^{1/4}=200$ (short-dashed line) and 211 MeV (long-dashed line).

$$Q_{CFL} = f_\pi^2 \mu_e \left(1 - \frac{m_\pi^4}{\mu_e^4}\right). \tag{4.7}$$

In the above thermodynamic potential, we have neglected the contribution due to the kaon condensation which is an effect of order m_s^4 and thereby small compared to the$\Delta^2\mu_q^2$ contribution to the thermodynamic potential for $\Delta \sim 100$ MeV.

V. MIXED PHASE AND HYBRID STAR PROPERTIES

We now consider the scenario of a mixed phase of hadronic and quark matter. In the mixed phase charge neutrality is imposed globally, i.e., the quark and hadronic phases are not neutral separately but rather the system prefers to rearrange itself so that

$$\chi\rho_c^{QP} + (1-\chi)\rho_c^{HP} + \rho_c^l = 0, \tag{5.1}$$

where ρ_c^{QP} and ρ_c^{HP} are the charge densities of quark and hadron phases, χ is the volume fraction occupied by the quark phase, $(1-\chi)$ is the volume fraction occupied by the hadron phase, and ρ_c^l is the lepton charge density. As usual, the phases boundary of the coexistence region between the hadron and quark phases is determined by the Gibbs criteria. The critical pressure and critical neutron and electron chemical potentials are determined by the conditions

$$\mu_{HP,i} = \mu_{QP,i} = \mu_i,\ i = n,e,\ T_{HP} = T_{QP},$$
$$P_{HP}(\mu_{HP},T) = P_{QP}(\mu_{QP},T),$$

reflecting the needs of chemical, thermal, and mechanical equilibrium, respectively. The energy density and the total baryon density in the mixed phase read

$$\varepsilon = \chi\varepsilon^{QP} + (1-\chi)\varepsilon^{HP} + \varepsilon^l, \tag{5.2}$$

$$\rho = \chi\rho^{QP} + (1-\chi)\rho^{HP}. \tag{5.3}$$

Notice that in all equations above the quark phase (QP) can be either the UQM or the CFL phase. The EOS for the mixed phase are then constructed. Once they are obtained, the properties of the neutron stars can be computed. The equations for the structure of a relativistic spherical and static star composed of a perfect fluid were derived from Einstein's equations by Oppenheimer and Volkoff [33]. They are

$$\frac{dP}{dr} = -\frac{G}{r}\frac{[\varepsilon+P][M+4\pi r^3 P]}{(r-2GM)}, \tag{5.4}$$

$$\frac{dM}{dr} = 4\pi r^2 \varepsilon, \tag{5.5}$$

with G as the gravitational constant and $M(r)$ as the enclosed gravitational mass. We have used $c=1$. Given an EOS, these equations can be integrated from the origin as an initial value problem for a given choice of the central energy density (ε_0). The value of $r(=R)$, where the pressure vanishes defines the surface of the star. We solve the above equations to study the structural properties of the star, using the EOS derived above.

VI. RESULTS AND DISCUSSION

In all figures shown, set (a) for the meson-hyperon coupling constants was used, unless stated otherwise. We have omitted all results for the parameter sets (b) and (c) because they are very similar to the ones obtained with set (a). Actually, all differences appear only in the hadron phase at densities where the mixed phase is already the dominant one. It is worth emphasizing that, as stated in Secs. III and IV, the u and d quark masses are different in the UQM and CFL models.

In Figs. 2(a) and 2(b) the EOS obtained with the unpaired quark model and the color-flavor locked phase are displayed for different values of the bag pressure B. The onset of the mixed phase and quark pure phase occurs at lower densities for smaller values of B. This effect has already been discussed in Ref. [34] for the UQM description. A smaller value of B gives a softer EOS in the mixed phase because the onset of the mixed phase occurs at lower densities. However at higher densities, after the onset of the quark phase it becomes harder. The mixed phase shrinks with the decrease of the B parameter in both quark models. This fact can be also observed in Table II, where the beginning and ending energy densities of the mixed phase are displayed in the last two columns. For the CFL, no mixed phase was found for $B^{1/4}=180$ MeV with $m_s=150$ MeV and $\Delta=100$ MeV, giving rise to a pure quark matter star. For the sake of comparison we have plotted the EOS for the same bag pressure for the UQM and CFL phase in Fig. 3. We include in the same figure the EOS obtained with NLWM plus UQM (short-dashed line).

TABLE II. Mixed star properties.

Model	$B^{1/4}$ (MeV)	$M_{max}/M_{\odot}$	ε_0 (fm^{-4})	ε_{min} (fm^{-4})	ε_{max} (fm^{-4})
QMC+UQM	180	1.41	8.53	1.26	5.24
QMC+UQM	190	1.58	5.52	1.63	7.02
QMC+UQM	200	1.73	4.85	2.05	8.74
QMC+UQM	210.854	1.85	4.68	2.73	10.57
QMC+CFL	190	1.32	12.56	1.35	4.56
QMC+CFL	200	1.49	3.31	1.92	6.25
QMC+CFL	211.303	1.76	3.94	2.66	8.28
NLWM+UQM	180	1.40	7.38	1.17	4.62
NLWM+UQM	190	1.64	4.58	1.81	6.06

One can see from this figure and Table II that the mixed phase in the CFL appears and ends at lower energy densities than in the UQM. This result has the same qualitative behavior as the ones shown in Ref. [17]. Comparing QMC and NLWM with UQM one can see that they behave similarly at low densities. For $\epsilon > 4.5$ fm^{-4} the NLWM-EOS becomes softer in the mixed phase. This is due to the fact that at higher densities the NLWM with hyperons becomes softer than the QMC-EOS, Fig. 1.

In Fig. 4 the particle population for the baryons, leptons, and quarks are shown for the UQM and different bag pressures and for the CFL with one chosen bag value. Hyperons only appear if the bag constant is very high, in our case $B^{1/4}=210.85$ MeV . This value corresponds to the B_B value of the bag used in the QMC model for the hadronic phase. A different behavior was obtained with NLWM in Ref. [25]

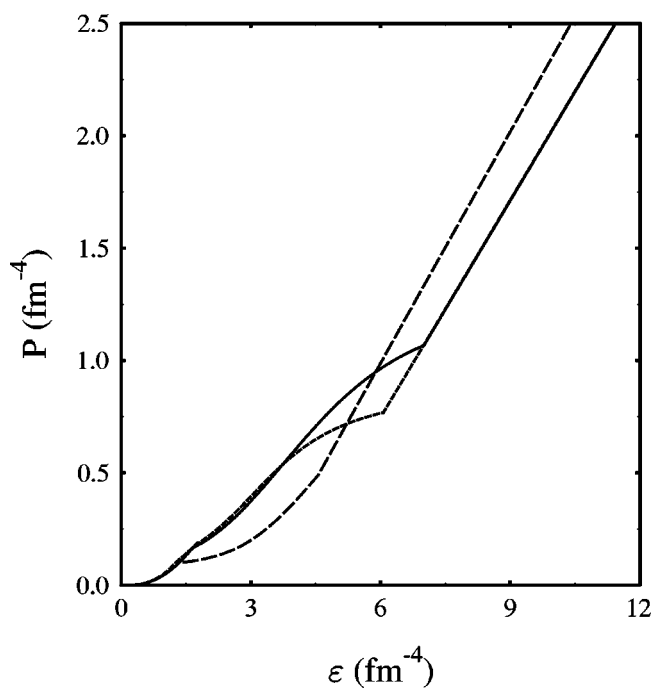

FIG. 3. EOS obtained with QMC plus UQM (solid line), QMC plus CFL (dashed line), and NLWM plus UQM (dotted line) with $B^{1/4}=190$ MeV. Only here we have considered $m_u=m_d=0$ MeV in both QMC models to compare the equations of state.

where the hyperons are present both for $B^{1/4}=180$ and 190 MeV. As already discussed, both the mixed phases and the quark phase appear at lower densities for lower B values. For the CFL phase and $B^{1/4}=200$ MeV, the quarks appear at 2.67 nuclear saturation density. In Ref. [17], for a bag pressure of $B^{1/4}=190$ MeV, the quarks appear at 2.149 ρ_0. We can see that our results are compatible with the ones shown there, obtained within a NLWM formalism with $K=240$ MeV and $M^*=0.78M$. While in Fig. 4(c), u,d, and s quark populations come out different, in Fig. 4(d), because of the imposition of equal quark densities in the CFL model, they are forced to be equal. Also, the e^- population, which disappears at the onset of the quark phase in all the EOS studied, in the CFL model, goes to zero at a much lower density than in the UQM model, because the onset of a pure quark phase occurs at lower densities.

As already discussed in Refs. [25,26], the presence of strangeness in the core and crust of neutron and proto-neutron stars has important consequences in understanding some of their properties. In Fig. 5 we show the strangeness fraction defined as

$$r_s = \chi r_s^{QP} + (1-\chi) r_s^{HP} \tag{6.1}$$

with

$$r_s^{QP} = \frac{\rho_s}{3\rho}, \quad r_s^{HP} = \frac{\sum_B |q_s^B| \rho_B}{3\rho},$$

where q_s^B is the strange charge of baryon B, for the different models discussed in this work. In all cases the strangeness fraction rises steadily. If the UQM is used, at the onset of the pure quark phase it has reached 30% of the baryonic matter. Although the amount of strangeness varies in the mixed phase, it is the same in the pure quark phase independent of the model used to describe the hadron phase. Nevertheless, if the CFL model is used for the quark phase, as a result of the equal quark densities imposition, the strangeness content reaches 1/3 of the total baryonic matter. Comparing QMC and NLWM with UQM, we conclude the strangeness content increases faster when the NLWM is used. This is due to the fact that in this model the hyperons also contribute.

In Table II we show the values obtained for the maximum mass of a neutron star as a function of the central density for

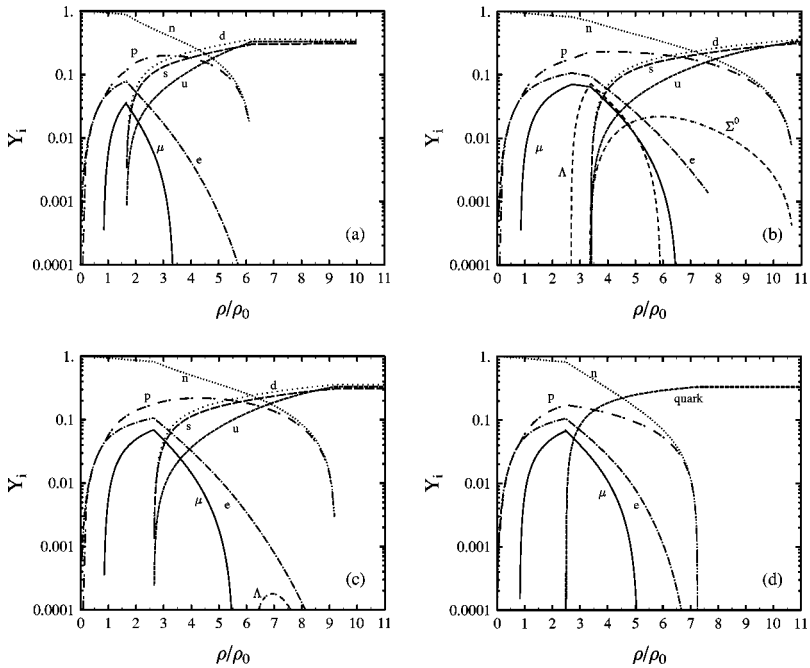

FIG. 4. Particle fractions $Y_i = \rho_i/\rho$ for i= baryons, leptons, and quarks, obtained with the QMC+UQM (a) for $B^{1/4}=180$ MeV, QMC+UQM (b) for $B^{1/4}=210.85$ MeV, QMC+UQM (c) for $B^{1/4}=200$ MeV, and QMC+CFL (d) for $B^{1/4}=200$ MeV.

some of the EOS studied in this work with UQM and CFL. Different bag parameters are used. We can see that the maximum mass of the star increases and its central energy decreases with increasing B. This result agrees with the fact that a larger B value corresponds to a harder EOS at high densities as shown in Fig. 2. For $B^{1/4}=180$ MeV(QMC+UQM) and $B^{1/4}=190$ MeV(QMC+CFL), the central density of the star lies outside of the range of the mixed phase, which is an indication of a star with a quark core. In the last case we get a very high central density due to the very soft EOS this parametrization gives rise to. In fact the predicted maximum mass for a hybrid star within this parametrization is too low as discussed below. In all the other cases discussed the central density of the star is always within the mixed phase. We have also added some results obtained with the nonlinear Walecka model [25] instead of the QMC for the hadron phase for the sake of comparison. For the same B, the maximum mass is about the same, the central core is also made up of quarks, and the mixed phase starts and finishes at lower densities. In Ref. [17], the authors have found maximum masses around $1.6M_\odot$ for maximum B values of $B^{1/4}=185$ MeV. For these B values, our results come out at the same order.

The radius of the maximum mass star is sensitive to the low density EOS. In order to calculate the radius and to plot it versus the star mass, we have used the results of Baym, Pethick, and Sutherland [35] for low baryonic densities.

In Fig. 6 the mass of the family of stars obtained with QMC is plotted in terms of their radii for both quark models used and $B^{1/4}=190$ and 200 MeV. We also include the family of stars obtained with NLWM plus UQM with $B^{1/4}=190$ MeV. The radii of the stars within QMC are 11.95 Km ($B^{1/4}=190$ MeV) and 12.47 Km ($B^{1/4}=200$ MeV) for UQM and 8.79 Km ($B^{1/4}=190$ MeV) and 13.31 Km ($B^{1/4}=200$ MeV) for CFL. For the NLWM family of stars we get $R=12.53$ Km ($B^{1/4}=190$ MeV). Some conclusions can be drawn. Comparing QMC and NLWM for $B^{1/4}=190$ MeV, the maximum mass of a stable star is similar for both models. The fact that NLWM-$M_\odot$ is larger shows that the main contribution to the star comes from the less dense regions, where the NLWM-EOS is harder than the QMC-EOS (see Fig. 3). We consider now the families of stars obtained within QMC for both B values using UQM and CFL. The quark contribution becomes more important for the smaller B values mainly for the CFL results. In particular, for $B^{1/4}=190$ MeV we get a quite small maximum

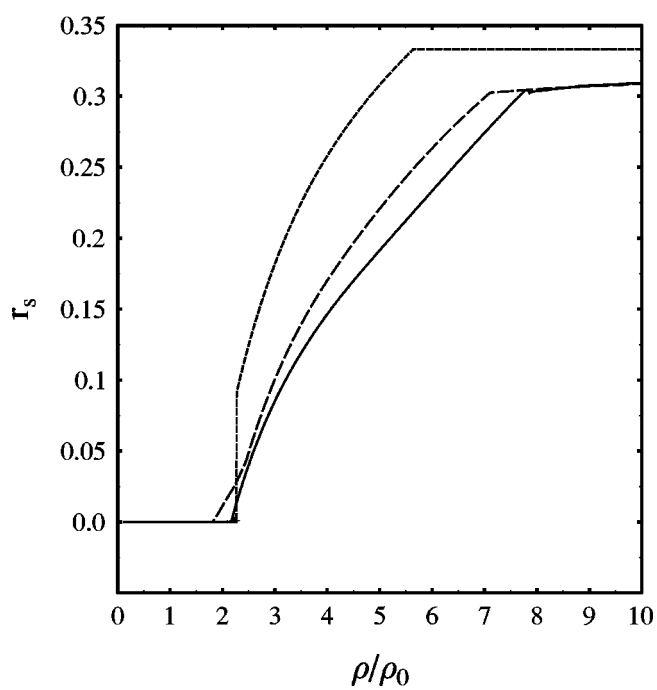

FIG. 5. Strangeness content obtained with QMC plus UQM (solid line), QMC plus CFL (dotted line), and NLWM plus UQM (dashed line) for $B^{1/4}=190$ MeV.

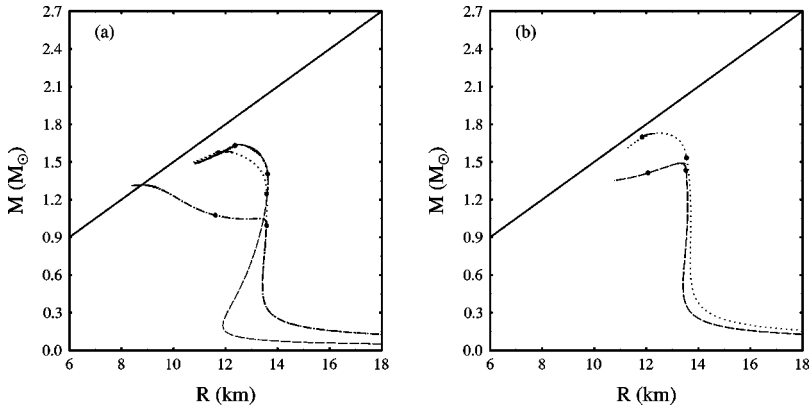

FIG. 6. Neutron star mass vs radius obtained with the (a) QMC plus UQM (solid line), QMC plus CFL (dotted line), and NLWM plus UQM (long-dashed line) for $B^{1/4}=190$ MeV; (b) QMC plus UQM (dotted line) and QMC plus CFL (dashed line) for $B^{1/4}=200$ MeV. The dots indicate the beginning and end of the mixed phases.

$M_\odot$ and a corresponding small radius. A maximum mass of 1.32 $M_\odot$ is too small for accounting for the presently known radio-pulsar masses [36], even after corrections due to rotation. Similar numbers were obtained with the NLWM plus CFL in Ref. [17] for slightly different values of B and m_s. In fact, since these maximum mass stars have a small hadron exterior region the properties of the star are mainly determined by the quark model used. It is also clear from Fig. 6 that the star properties are sensitive to the B value, in particular within the CFL formalism. Taking $B^{1/4}=200$ MeV the contribution of the mixed phase to stable stars is much smaller, restricted to the core of the star. In Fig. 6(b) the properties of the stars which only contain hadronic matter do not coincide because we have taken $m_u=m_d=5.5$ MeV for the QMC parametrization for the results QMC plus UQM and zero otherwise.

A straightforward method of determining neutron star properties is by measuring the gravitational redshift of spectral lines produced in neutron star photosphere which provides a direct constraint on the mass-to-radius ratio. Recently a redshift of 0.35 from three different transitions of the spectra of the x-ray binary EXO0748-676 was obtained in Ref. [37]. This redshift corresponds to $M_\odot/R(km)=0.15$. In Fig. 6 we have added the line corresponding to this constraint, and only the EOS for QMC plus CFL with $B^{1/4}=190$ MeV barely satisfies this constraint. In fact, the above constraint excludes all the EOS with hyperons, quarks, or obtained within a relativistic mean-field approach, as compiled in Ref. [38].

VII. CONCLUSIONS

In the present paper we have studied the EOS for neutron stars using both the unpaired quark matter based on the MIT bag model and the CFL phase for describing the quark phase and a relativistic mean-field quark-meson coupling description in which quarks interact via the exchange of σ, ω, and ρ mesons for the hadron phase.

We have compared the results obtained within the QMC model with the ones obtained within the NLWM. For similar properties at nuclear saturation we conclude that contrary to NLWM, with the QMC the hyperons only appear for a very high value of the bag constant. Also hyperons make the NLWM-EOS much softer than the QMC-EOS. For the hyperon-meson couplings we have used three choices and verified that they did not have any effect on the onset of hyperons. The none appearance of hyperons affects the variation of the strangeness content of the star with density: except for the quark phase we get higher fractions with the NLWM.

For the bag pressure parameter B we have used three different values, which produce different EOS and consequently the properties of the stars are dependent on them. Small B values give stable stars with a quark core. However, for a given gap constant Δ we obtain a phase transition to a deconfined CFL phase only if B is greater than a critical value. For lower values we get an EOS of pure quark matter and pure quark matter stars. For $\Delta=100$ MeV we should have $B^{1/4}\geqslant 185$ MeV. For $B^{1/4}=190$ MeV and $m_s=150$ MeV, with QMC plus CFL we are not able to obtain stable stars with masses equal to most of radio-pulsar masses known. We have also shown that just one of the EOS we have studied satisfies the constraint imposed by the recently measured redshift of 0.35 from three different transitions of the spectra of the x-ray binary EXO0748-676 [37].

We have concluded that the EOS in QMC is so soft that hyperons would only make the EOS softer at densities for which the EOS has already been softened by the presence of quarks, except if we take a quite hard quark matter EOS. A direct consequence is that the appearance of a strange phase only occurs with the onset of the mixed phase. For the EOS with a CFL phase there is even a steep jump on the strangeness fraction from zero to almost 0.1 and the strangeness fraction rises faster than in the quark unpaired phase. It has been shown in different cases that newly born star with a strange phase supports more mass than a cold one [19,34] giving rise to a retarded collapse to a black hole. We may expect a similar mechanism in the present situation. The *radiation radius* defined as $R_\infty=R/\sqrt{1-2M/R}$, obtained by redshifting the stars luminosity and temperature [38], is a measurable quantity which imposes restrictions on the acceptable EOS for stellar matter; namely, $R<R_\infty$ must be satisfied. Except for the EOS obtained with QMC plus CFL for $B^{1/4}=190$ MeV, all the other EOSs studied in the present work would be excluded if a radiation radius $R_\infty<14$ km would be measured. In conclusion, the EOSs obtained within the QMC model for hadronic matter plus a quark phase will only satisfy the recent measurement of the gravitational redshift of spectral lines produced in the neutron star photosphere for a particular choice of the parameters and with a CFL phase.

Further measurements may impose further constraints. As most relativistic models the QMC and bag models are also parameter dependent. A more systematic study has to be done in order to verify whether a set of acceptable parameters for the QMC+ MIT bag model gives a family of stars which contains the measured value.

In Ref. [5], strange meson fields, namely, the scalar meson field $f_0(975)$ and the vector meson field $\phi(1020)$, were also considered in order to reproduce the observed strongly attractive $\Lambda\Lambda$ interaction. They have shown that the introduction of these strange mesons makes the EOS harder due to the repulsive effect of the $\phi(1020)$, meson. A harder EOS for the hadronic matter gives rise to an onset of the mixed phase at lower densities and a smaller mixed phase. The inclusion of these mesons and their influence on the properties of the stars are under investigation.

It has been shown that the effect of temperature on the maximum mass of stable stars is small compared to the effect of neutrino trapping [25,26,34]. Therefore, it would be interesting to include neutrino trapping even at $T=0$ MeV and impose leptonic number conservation in the models used here, and check the properties of the arising stars.

ACKNOWLEDGMENTS

This work was partially supported by CNPq (Brazil), CAPES (visiting researcher project), CAPES (Brazil)/GRICES (Portugal) under the Project No. 003/100, and FEDER/FCT (Portugal) under the Project No. POCTI/35308/FIS/2000.

[1] P. A. M. Guichon, Phys. Lett. B **200**, 235 (1988).
[2] K. Saito and A. W. Thomas, Phys. Lett. B **327**, 9 (1994); **335**, 17 (1994); **363**, 157 (1995); Phys. Rev. C **52**, 2789 (1995); P. A. M. Guichon, K. Saito, E. Rodionov, and A. W. Thomas, Nucl. Phys. **A601**, 349 (1996); K. Saito, K. Tsushima, and A. W. Thomas, *ibid.* **A609**, 339 (1996); Phys. Rev. C **55**, 2637 (1997); Phys. Lett. B **406**, 287 (1997).
[3] J. D. Walecka, Phys. Lett. B **83**, 491 (1974); B. D. Serot and J. D. Walecka, Adv. Nucl. Phys. **16**, 1 (1986).
[4] K. Tsushima, K. Saito, J. Haidenbauer, and A. W. Thomas, Nucl. Phys. **A630**, 691 (1998).
[5] S. Pal, M. Hanauske, I. Jakout, H. Stöcker, and W. Greiner, Phys. Rev. C **60**, 015802 (1999).
[6] P. G. Blunden and G. A. Miller, Phys. Rev. C **54**, 359 (1996); N. Barnea and T. S. Walhout, Nucl. Phys. **A677**, 367 (2000); H. Shen and H. Toki, Phys. Rev. C **61**, 045205 (2000); P. K. Panda, R. Sahu, and C. Das, *ibid.* **60**, 38 801 (1999); P. K. Panda, M. E. Bracco, M. Chiapparini, E. Conte, and G. Krein, *ibid.* **65**, 065206 (2002); P. K. Panda and F. L. Braghin, *ibid.* **66**, 055207 (2002).
[7] P. K. Panda, A. Mishra, J. M. Eisenberg, and W. Greiner, Phys. Rev. C **56**, 3134 (1997); I. Zakout and H. R. Jaqaman, *ibid.* **59**, 962 (1999).
[8] G. Krein, D. P. Menezes, M. Nielsen, and C. Providencia, Nucl. Phys. **A674**, 125 (2000); P. K. Panda, G. Krein, D. P. Menezes, and C. Providencia, Phys. Rev. C **68**, 015201 (2003).
[9] X. Jin and B. K. Jennings, Phys. Lett. B **374**, 13 (1996); Phys. Rev. C **54**, 1427 (1996).
[10] H. Mueller and B. K. Jennings, Nucl. Phys. **A640**, 55 (1998); **A626**, 966 (1997).
[11] C. H. Johnson, D. J. Horen, and C. Mahaux, Phys. Rev. C **36**, 2252 (1987).
[12] A. Chodos, R. L. Jaffe, K. Johnson, C. B. Thorne, and V. F. Weisskopf, Phys. Rev. D **9**, 3471 (1974).
[13] B. Freedman and L. McLerran, Phys. Rev. D **17**, 1109 (1978).
[14] E. Farhi and R. L. Jaffe, Phys. Rev. D **30**, 2379 (1984).
[15] J. I. Kapusta, *Finite Temperature Field Theory* (Cambridge University Press, Cambridge, 1989).
[16] I. Shovkovy, M. Hanauske, and M. Huang, Phys. Rev. D **67**, 103004 (2003).
[17] M. Alford and S. Reddy, Phys. Rev. D **67**, 074024 (2003).
[18] M. Buballa and M. Oertel, Nucl. Phys. **A703**, 770 (2002); M. Baldo, M. Buballa, G. F. Burgio, F. Neumann, M. Oertel, and H.-J. Schulze, Phys. Lett. B **562**, 153 (2003).
[19] A. W. Steiner, S. Reddy, and M. Prakash, Phys. Rev. D **66**, 094007 (2002).
[20] M. Alford, K. Rajagopal, S. Reddy, and F. Wilezeck, Phys. Rev. D **64**, 074017 (2001).
[21] K. Rajagopal and F. Wilezeck, Phys. Rev. Lett. **86**, 3492 (2001).
[22] M. G. Alford, Annu. Rev. Nucl. Part. Sci. **51**, 131 (2001).
[23] A. Burrows and J. M. Lattimer, Astrophys. J. **307**, 178 (1986).
[24] W. Keil and H.-Th. Janka, Astron. Astrophys. **296**, 145 (1995).
[25] D. P. Menezes and C. Providência, Phys. Rev. C **68**, 035804 (2003).
[26] D. P. Menezes and C. Providência, nucl-th/0312050.
[27] Y. Nambu and G. Jona-Lasinio, Phys. Rev. **122**, 345 (1961); **124**, 246 (1961).
[28] R. E. Chrien and C. B. Dover, Annu. Rev. Nucl. Part. Sci. **39**, 113 (1989).
[29] S. A. Moszkowski, Phys. Rev. D **9**, 1613 (1974).
[30] N. K. Glendenning and S. Moszkowski, Phys. Rev. Lett. **67**, 2414 (1991).
[31] N. K. Glendenning, *Compact Stars* (Springer-Verlag, New York, 2000).
[32] D. Son and M. Stephanov, Phys. Rev. D **61**, 074012 (2000); **62**, 059902(E) (2000).
[33] R. C. Tolman, Phys. Rev. **55**, 364 (1939); J. R. Oppenheimer and G. M. Volkoff, *ibid.* **55**, 374 (1939).
[34] M. Prakash, I. Bombaci, M. Prakash, P. J. Ellis, J. M. Lattimer, and R. Knorren, Phys. Rep. **280**, 1 (1997).
[35] G. Baym, C. Pethick, and P. Sutherland, Astrophys. J. **170**, 299 (1971).
[36] S. E. Thorsett and D. Chakrabarty, Astrophys. J. **512**, 288 (1999).
[37] J. Cottam, F. Paerels, and M. Mendez, Nature (London) **420**, 51 (2002).
[38] J. M. Lattimer and M. Prakash, Astrophys. J. **550**, 426 (2001).